RFID Modeling, Characterization, and Optimization

by

Joseph A. Cudrnak

Senior Project

ELECTRICAL ENGINEERING DEPARTMENT

California Polytechnic State University

San Luis Obispo

December 2009

TABLE OF CONTENTS

Section *Page*

Acknowledgements……..iv

I. Abstract……1

II. Background...……..2

III. RFID Characterization……...3

IV. RFID Modeling……12

V. Design Modeling and Optimization……...19

VI. Conclusions and Recommendations……..……...26

VII. Continued Research……..……...…27

VIII.

References……..……..28

Appendices

A. Parts List……29

B. Schedule…….30

LIST OF TABLES AND FIGURES

Tables

1. Omni ID Tag Types and Datasheet Values ..……...5

2. Tag Minimum Read Distance….……..9

3. Design Modeling Results……25

Figures

1. Omni ID Prox Label Tag on Conductive Plate……....3

2. Transmit and Receive Patch Antennas……4

3. E and H Plane Reference Angles for Measured Data…….……5

4. H-Plane Maximum Attenuation Plot for the Alien Squiggle Tag……5

5. H-Plane Maximum Attenuation Plot for the Alien Squiggle Tag……6

6. E-Plane Maximum Attenuation Plot for three Omni ID Tags……..6

7. H-Plane Maximum Attenuation Plot for three Omni ID Tags…….7

8. Maximum Read Distance in the H plane……10

9. Maximum Read Distance in the E Plane……10

10. HFSS Model of Wave Zero RFID Tag……..……...…12

11. Simulated $|S_{11}|$ Plot of Wave Zero RFID Tag……..……..…13

12. Simulated radiation pattern of Wave Zero RFID Tag…….…..14

13. HFSS Model of Alien Squiggle RFID Tag……...14

14. Simulated $|S_{11}|$ of Alien Squiggle RFID Tag……...15

15. Simulated radiation pattern of Alien Squiggle RFID Tag…….16

16. HFSS Model of Wave Zero Tag on Dielectric on Conductive Plate……17

17. Simulated $|S_{11}|$ for Wave Zero Tag on Dielectric on Conductive Plate……..…..17

18. Radiation Pattern for Wave Zero Tag on Dielectric on Conductive Plate……18

19. HFSS Model of Base Design…….19

20. Simulated radiation pattern for Base Design with associated |E| values……...20

21. Reflection path through cross section of Design 1……21

22. HFSS Model of Design 1……..21

23. Simulated Radiation Pattern of Design 1……..22

24. HFSS Model of Design 2…….…….23

25. Simulated Radiation Pattern of Design 2……..23

26. HFSS model of Design 3……...24

27. Simulated Radiation Pattern of Design 3……..25

Acknowledgements:

First of all, I would like to thank Dr. Arakaki for his support and guidance throughout the duration of the project. Also I would like to thank the people at Omni ID, Alien, and Wave Zero for their generous donations to the school, without which there would be no project to work on. And to the previous students who built the RF anechoic chamber on campus and designed the testing procedure for characterizing RFID tags. Their work was essential in establishing a basis with which I could continue research on RFID technology.

Abstract:

Passive RFID tags may be used to transmit a message to a reader. This technology is useful for many applications, including inventory systems. However, due to electromagnetic cancellation on conductive surfaces, the reader cannot detect RFID tags placed directly on conductive objects. Using tag characterization in an RF anechoic chamber and modeling in HFSS, three types of Omni ID tags were characterized and a design was proposed to maximize signal power delivered to the reader.

Background:

When electromagnetic radiation contacts a conductive plane, the signal is reflected and inverted. If a tag is placed directly on a conductive plane, this reflected signal adds destructively with direct tag radiation, cancelling the signal. However, if the tag is a quarter wavelength away from the conductive plane, the reflected signal adds constructively with direct radiation, maximizing the signal power delivered to the reader. At the tag operating frequency of 915 MHz, a quarter wavelength in air is 8.19 cm (3.224 in). Using a dielectric material, this length will be decreased, and the tag may be held a quarter wavelength away from the plate without being as physically obtrusive on the tagged object. One company, Omni ID offers an RFID product equipped with such a solution.

RFID Characterization:

First, a Lab View program was used to characterize the RFID tags in an RF anechoic chamber. This program records the number successful reads at a given direction, and increases the attenuation until the number of successful reads is zero, then increments the azimuth angle by a user defined value in degrees. This process is repeated over a range of user defined angles to plot the maximum signal attenuation as a function of direction. The measurement setup is shown in Figures 1 and 2. The motor shown in Figure 1 rotates to increment the azimuth angle. Figure 2 shows the transmitter and receiver patch antennas orientation. The reader sends out the carrier signal through the transmitter antenna. The signal is then rectified and modulated by the tag and sent back through the receiver antenna to the reader which demodulates the signal.

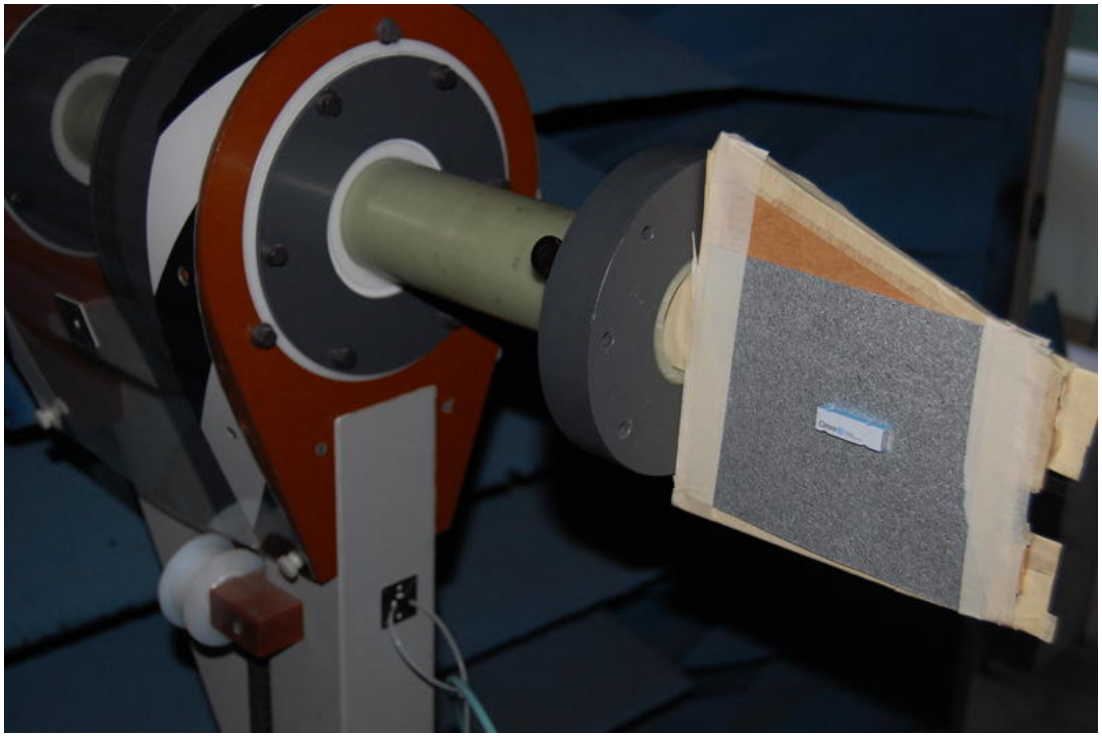

Figure 1: Omni ID Prox Label Tag on Conductive Plate

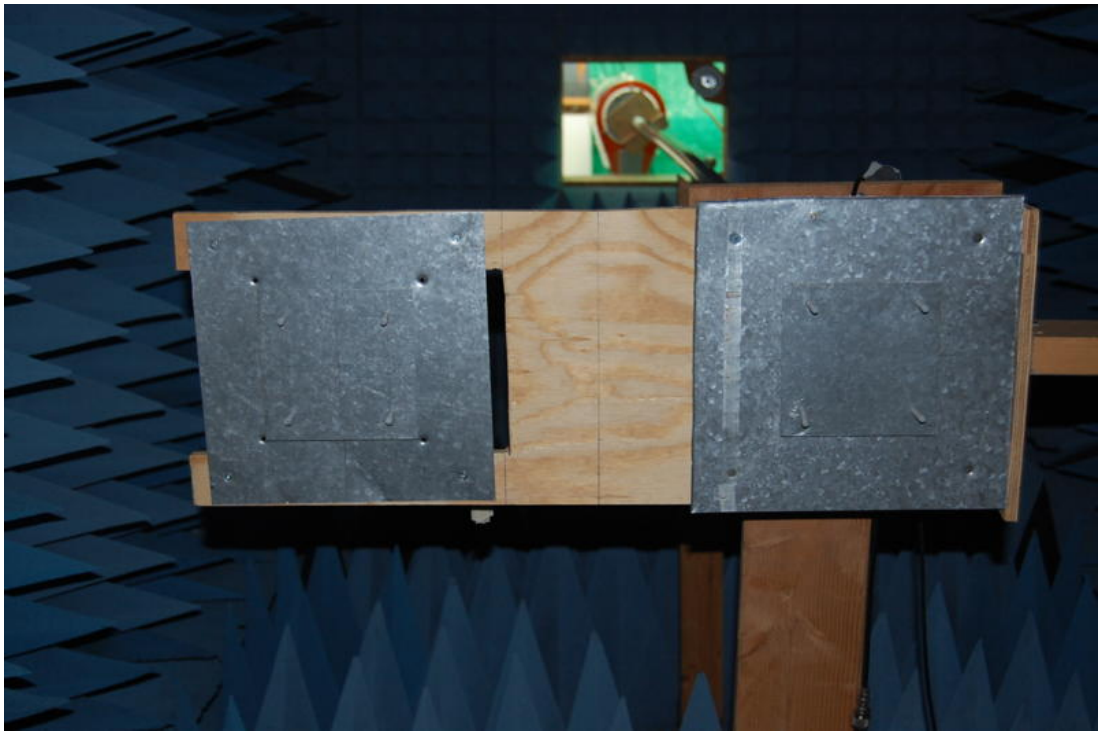

Figure 2: Transmit (left) and Receive (right) Patch Antennas.

The E plane is defined as a cross sectional plane of the radiation pattern in the direction of electric field intensity, while the H plane is defined as a cross sectional plane of the radiation pattern in the direction of magnetic field intensity. The motor shown in the background of Figure 2 rotates the fixture holding the antennas to measure the E or H plane. E and H plane measurements were taken for the Alien Squiggle tag, along with three types of Omni ID tags. Table 1 shows the types and sizes of Omni ID tags measured. The Omni ID tags were attached to a conductive plate as shown in Figure 1. The Alien Squiggle tag was attached to a piece of RF transparent cardboard. The measured data is shown in figures 4-7. Figure 3 shows the E and H plane reference angles with respect to tag orientation.

Omni ID Tag Type	Prox Label	Prox ABS	Flex Label
Tag Size (mm^3)	33 x 10 x 4.5	55 x 16 x 7.5	77 x 15 x 2.5
Read Distance	3 m	3 m	5 m

Table 1: Omni ID Tag Types and Datasheet Values

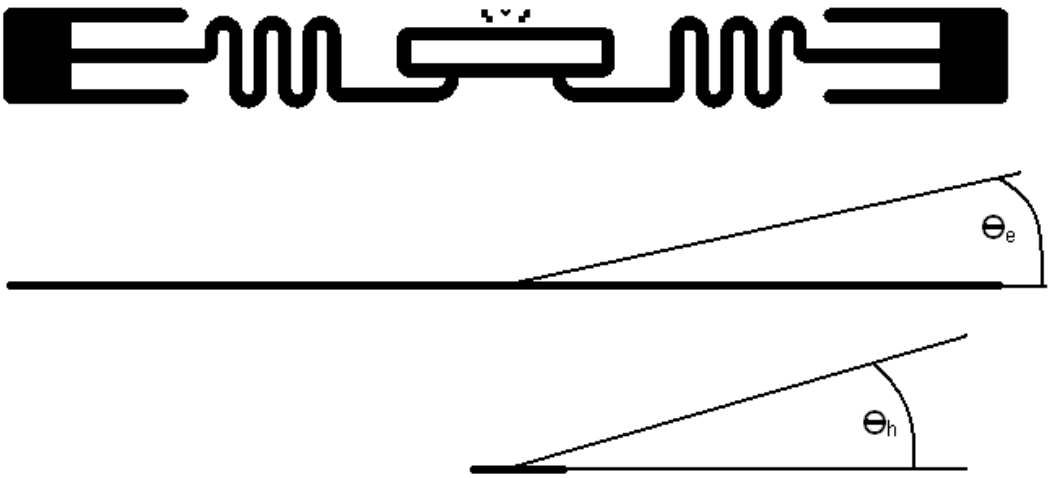

Figure 3: E and H Plane Reference Angles for Measured Data (wrt tag orientation)

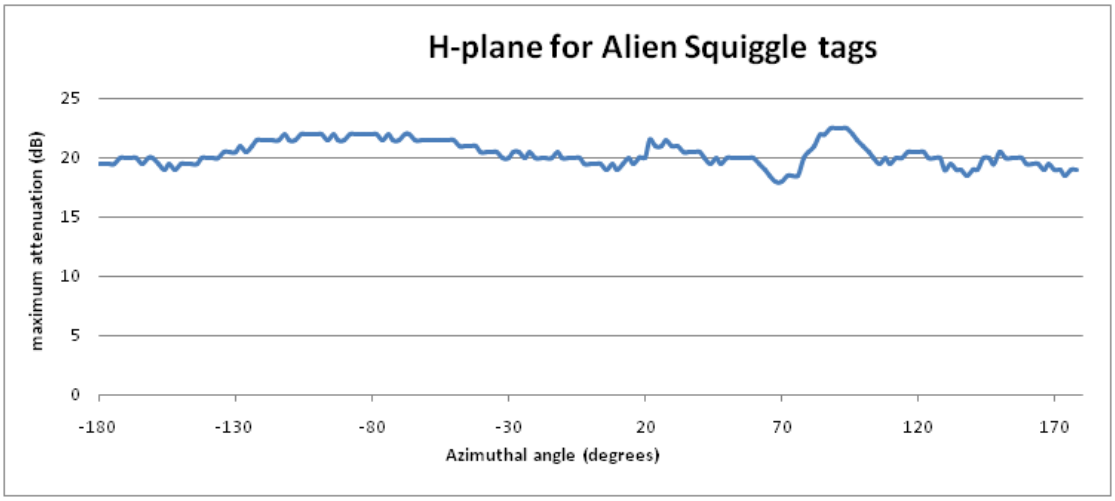

Figure 4: H-Plane Maximum Attenuation Plot for the Alien Squiggle Tag

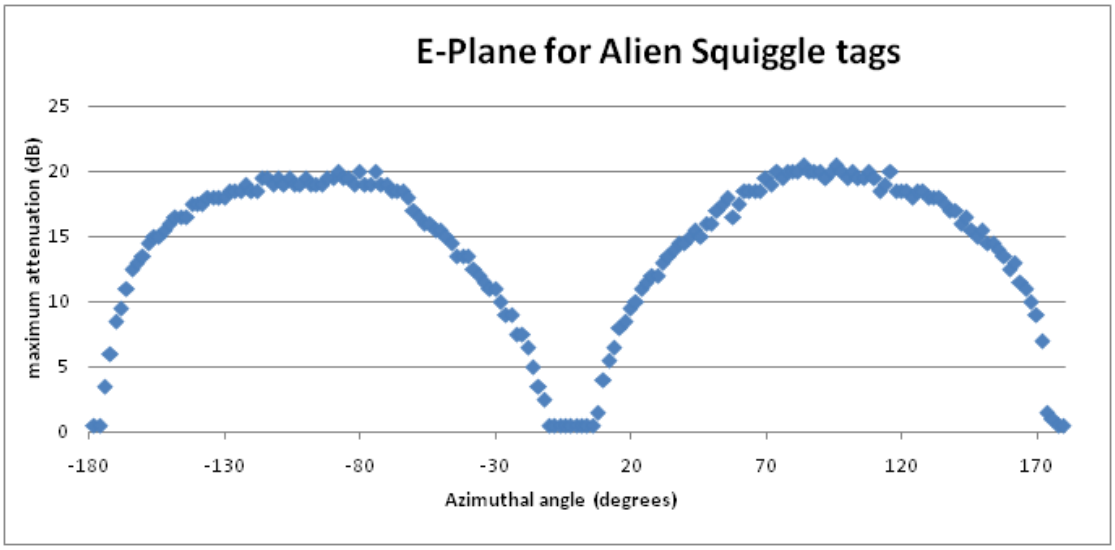

Figure 5: H-Plane Maximum Attenuation Plot for the Alien Squiggle Tag

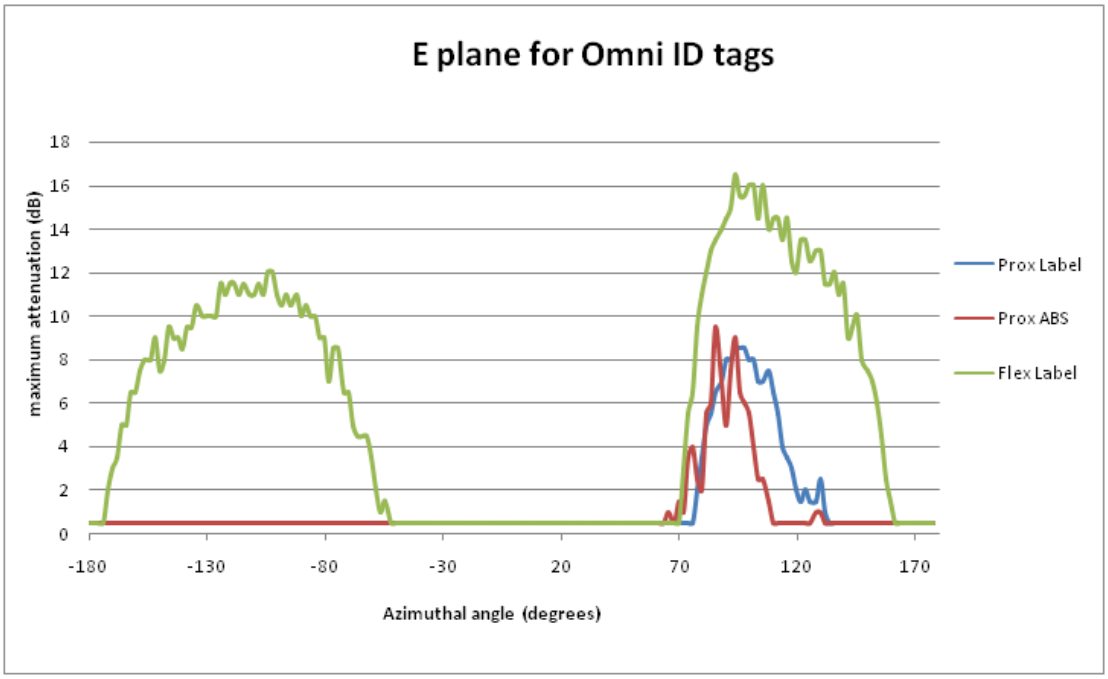

Figure 6: E-Plane Maximum Attenuation Plot for three Omni ID Tags.

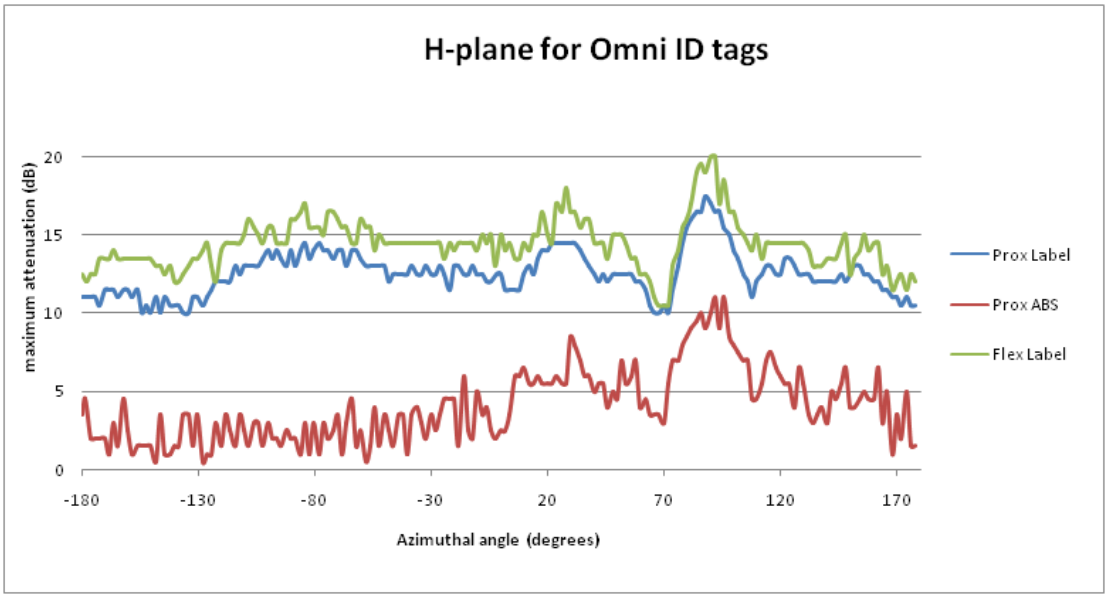

Figure 7: H-Plane Maximum Attenuation Plot for three Omni ID Tags.

Figures 4-7 show the maximum signal attenuation occurs around 90˚ in the E and H planes for each tag. In other words, maximum signal power is delivered to the reader when the tag is orthogonal to the reader antenna. Therefore, in applications with a fixed reader antenna and tag, this should be the orientation of the tag with respect to reader antenna.

The minimum read power of the Alien 9800 reader is -18 dBm. Because received signal power is proportional to attenuation, Figures 4-7 estimate the radiation pattern for each tag. The Alien 9800 reader transmit RF power is 0.5 watts or 27 dBm on the datasheet. The directivity of each tag could be determined from these data, and gain calculated for each tag based on an efficiency factor. However, the radiation efficiency cannot be calculated from these data because it involves calculation of losses in the dielectric material.

Using the Friis transmission formula:

$$1)\ \ P_{r1} = \frac{P_{t1} G_t G_r \lambda^2}{(4\pi R)^2}$$

Where:

$$P_{t1} = \ reader\ transmitted\ signal\ power$$

$$P_{r1} = \ tag\ received\ signal\ power$$

$$G_t = \ transmitter\ antenna\ gain = receiver\ antenna\ gain$$

$$G_r = \ tag\ antenna\ gain$$

$$R = \ read\ distance$$

The tag transmitted power is equal to the tag received power multiplied by efficiency factor epsilon:

$$2)\ \ P_{t2} = P_{r1} \times \epsilon$$

Using the Friis transmission formula again:

$$3)\ \ P_{r2} = \frac{P_{t2} G_t G_r \lambda^2}{(4\pi R)^2}$$

Where:

$$P_{t2} = \ tag\ transmitted\ signal\ power$$

Substitution yields:

$$4)\ \ P_{r2} = \frac{G_t G_r \lambda^2}{(4\pi R)^2} \times \epsilon \times \frac{P_{t1} G_t G_r \lambda^2}{(4\pi R)^2}$$

We can then rewrite the equation as:

$$5)\ \ P_{r2} = K \times \frac{P_{t1}}{R^4}$$

Where:

$$6)\quad K = \frac{(G_t\, G_r\, \lambda^2)^2 \epsilon}{(4\pi)^4}$$

Because P_{r2}, P_{t1}, and R are all known, we then may solve for the constant K as a function of signal attenuation or angle. Then solve for maximum read distance using the equation:

$$7)\quad R_{max} = \sqrt[4]{\frac{P_{t1} \times K}{P_{r_{min}}}}$$

Where:

$$P_{t1} = \ reader\ transmitted\ signal\ power\ = 33.01\ dBm$$

$$P_{r_{min}} = \ minimum\ received\ signal\ power\ = -18\ dBm$$

Table 2 shows the maximum read distance and value of K calculated for each tag, as well as the % difference between calculated values of R_{max} and the datasheet values shown in Table 1. These values are all calculated at the maximum, where the reader antenna is orthogonal to tag orientation. Figures 8 and 9 show the maximum read distance for each tag in the H and E planes.

Tag type	Max Attenuation	K	R_{max} (m)	% difference
Squiggle	22.5	0.01127	4.34557	N/A
Flex Label	20	0.006356	3.76534	-24.6
Prox Label	17.5	0.003566	3.2587	+8.62
Prox ABS	11	0.000798	2.2413	-25.29

Table 2: Tag Maximum Read Distance

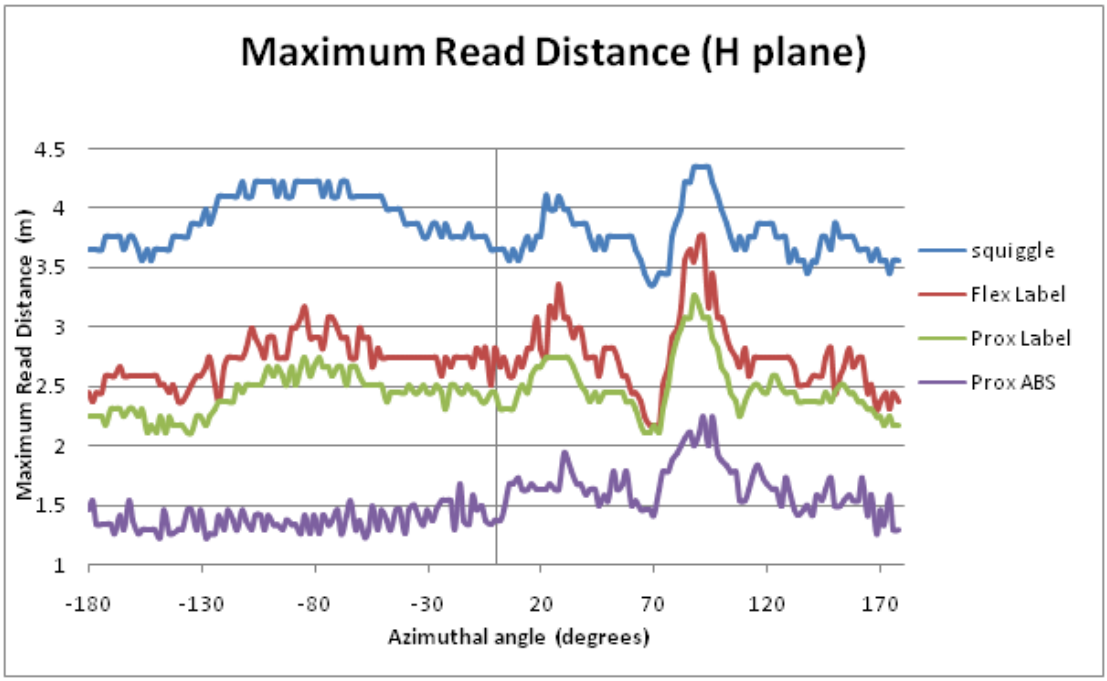

Figure 8: Maximum Read Distance in the H plane

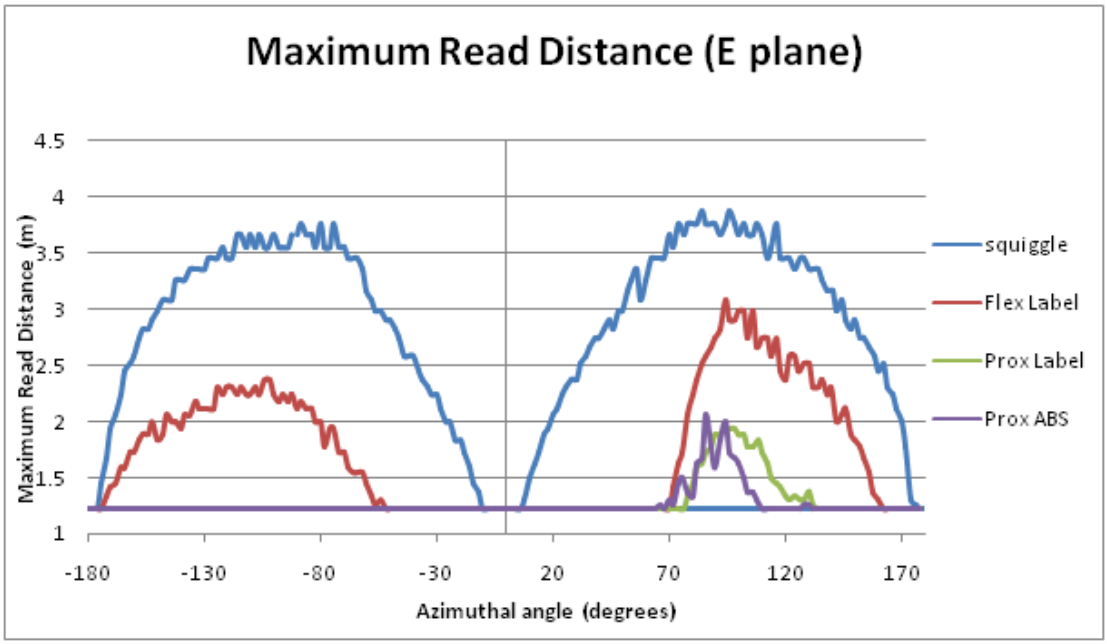

Figure 9: Maximum Read Distance in the E Plane

Note that maximum read distance values of 1.227 m may be inaccurate or even correspond to a signal null due to the limitations of the test. This is because the test had a minimum signal attenuation of 0.5 dB. A digital amplifier could be used in series as well as the attenuator to attain more accurate minimum read distance values.

RFID Modeling:

Two types of RFID tags were modeled in HFSS. The tags were measured using calipers and modeled in HFSS. The resulting model for the Wave Zero RFID tag is shown below in Figure 10.

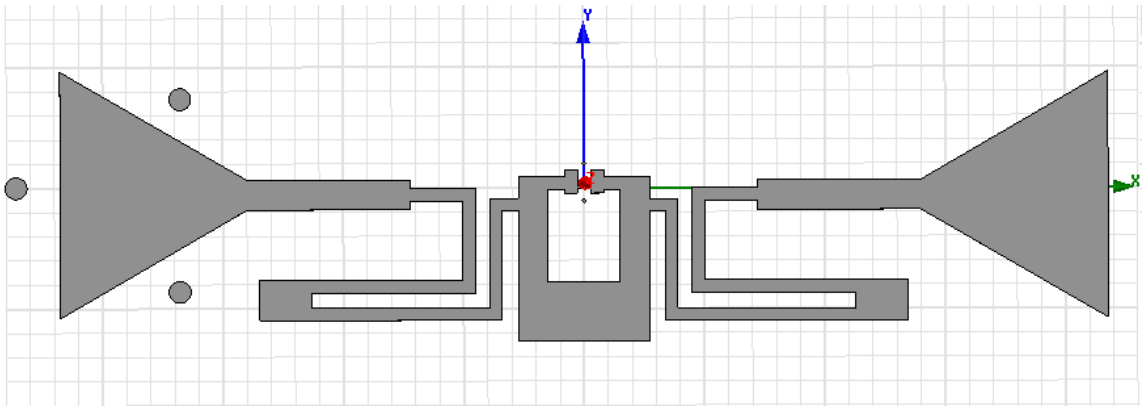

Figure 10: HFSS Model of Wave Zero RFID Tag

The simulated $|S_{11}|$ plot indicates a resonant frequency of 830 MHz, 9% below the tag carrier frequency of 915MHz. The model dimensions were scaled by 0.907 (frequency simulated/frequency desired) to increase the resonant frequency. The resulting $|S_{11}|$ plot is shown in Figure 11.

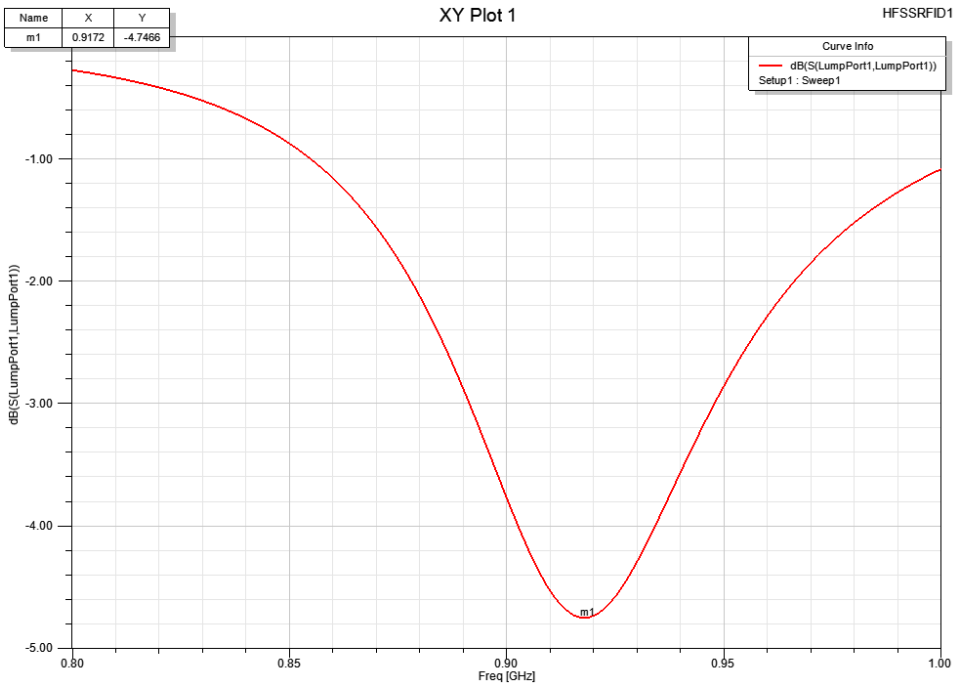

Figure 11: Simulated $|S_{11}|$ Plot of Wave Zero RFID Tag.

The resulting radiation pattern is shown in Figure 12. The radiation pattern shape toroidal, just like a dipole antenna. This substantiates the use of a dipole antenna to model the RFID tag in HFSS. Note that the null along the x axis corresponds to tag alignment.

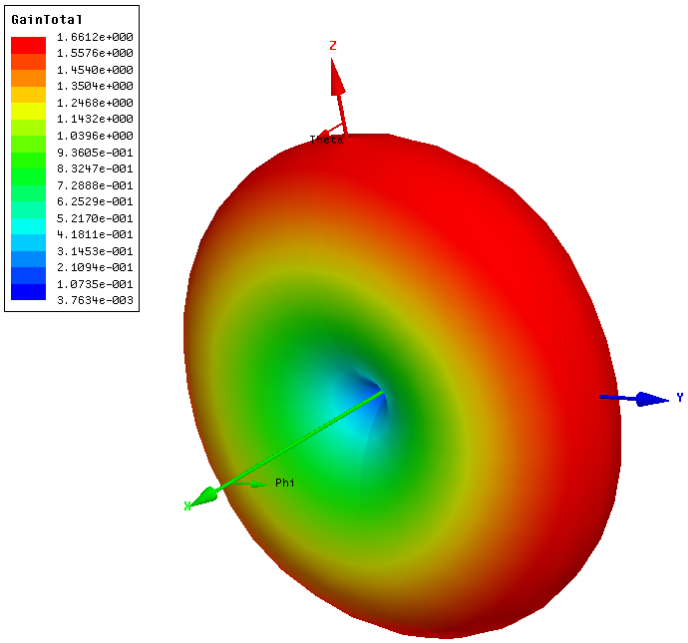

Figure 12: Simulated radiation pattern of Wave Zero RFID Tag.

Next, the Alien Squiggle tag was modeled in HFSS again measured using calipers. The resulting model is shown below in Figure 13.

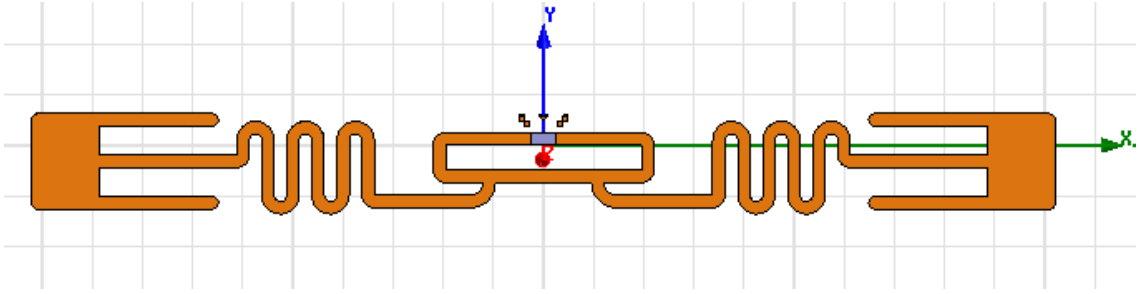

Figure 13: HFSS Model of Alien Squiggle RFID Tag

The simulated $|S_{11}|$ and radiation pattern plots for the Alien Squiggle tag are shown in figures 14 and 15 below. The resonant frequency was higher than expected by 9.2%, which required an increase in tag dimensions. This suggests that tag measurement was the source of error, or perhaps error in material assignment. Copper was chosen for the Squiggle tag while aluminum was used for the Wave Zero tag.

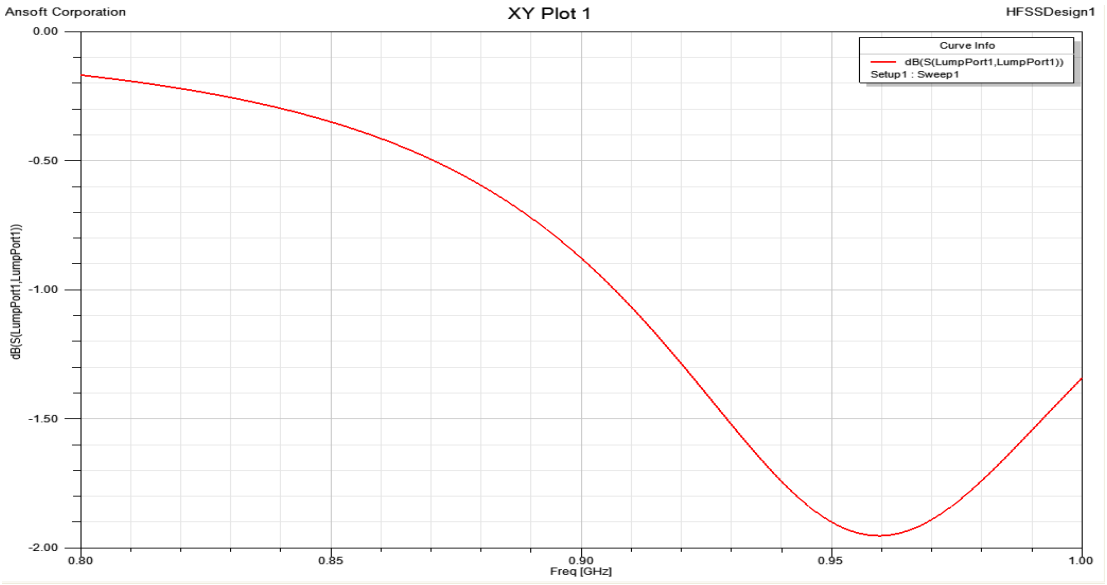

Figure 14: Simulated $|S_{11}|$ of Alien Squiggle RFID Tag

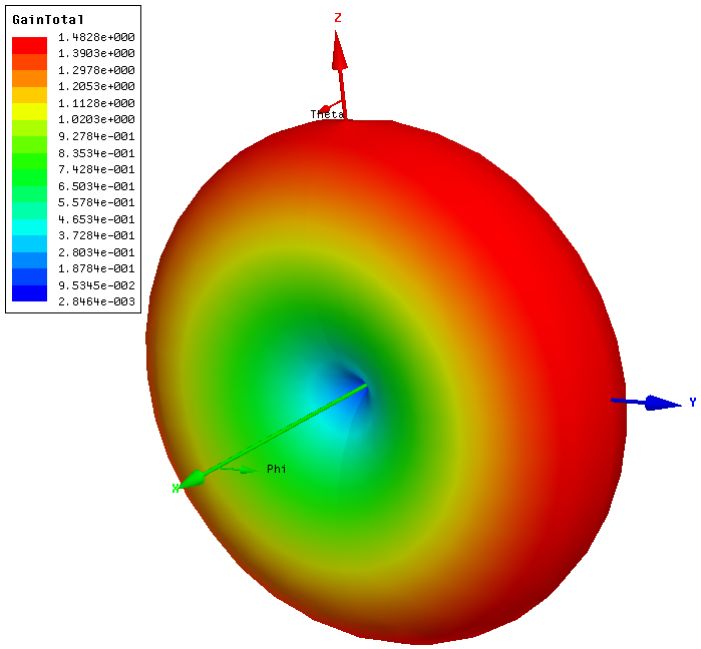

Figure 15: Simulated radiation pattern of Alien Squiggle RFID Tag

Next, the Wave Zero tag was modeled adjacent to a quarter wavelength dielectric material attached to a conductive plate as shown in Figure 16. The plate was arbitrarily assigned a width of 150 mm and a length of 100 mm. The resulting $|S_{11}|$ simulation is shown in Figure 17. The resonant frequency decreases with the addition of the dielectric and conductive plate, which is intuitive considering the addition of conductive material, or electrical length.

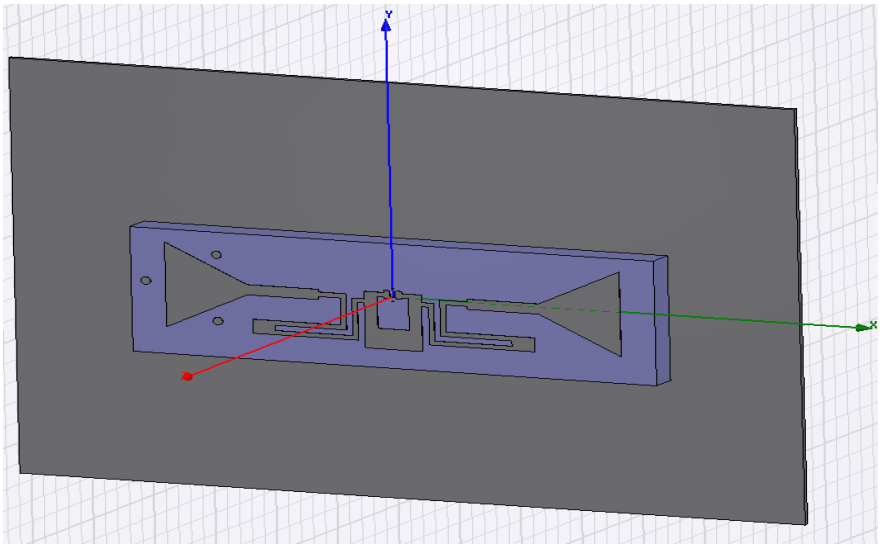

Figure 16: HFSS Model of Wave Zero Tag on Dielectric on Conductive Plate.

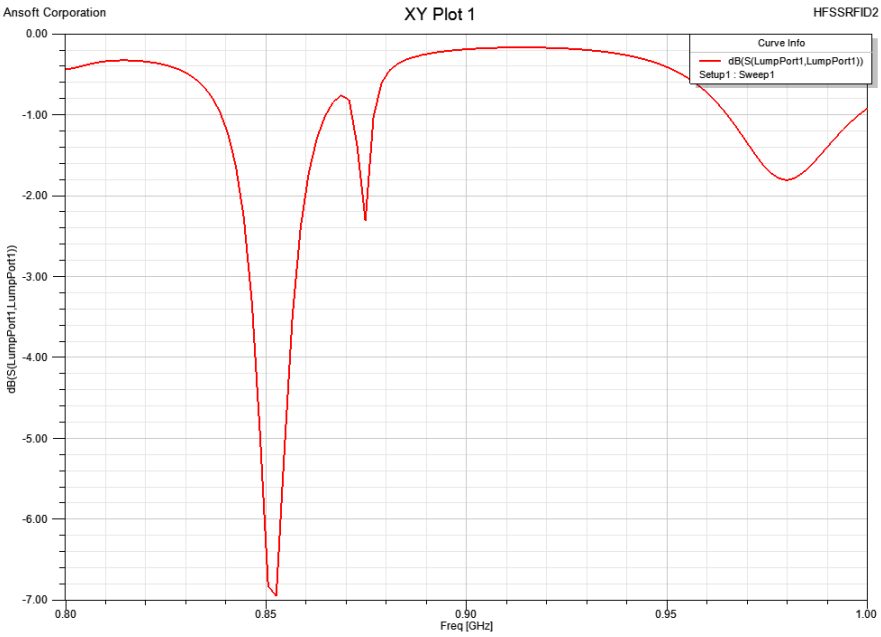

Figure 17: Simulated $|S_{11}|$ for Wave Zero Tag on Dielectric on Conductive Plate.

The conductive plate and dielectric material act as a ground plane and substrate, hence the model has a radiation pattern similar to that of a patch antenna. The simulated radiation pattern is shown in figure 18 below. Notice the increased directivity caused by the addition of dielectric material on conductive plate when compared to the toroidal pattern of the tag itself (Figure 12).

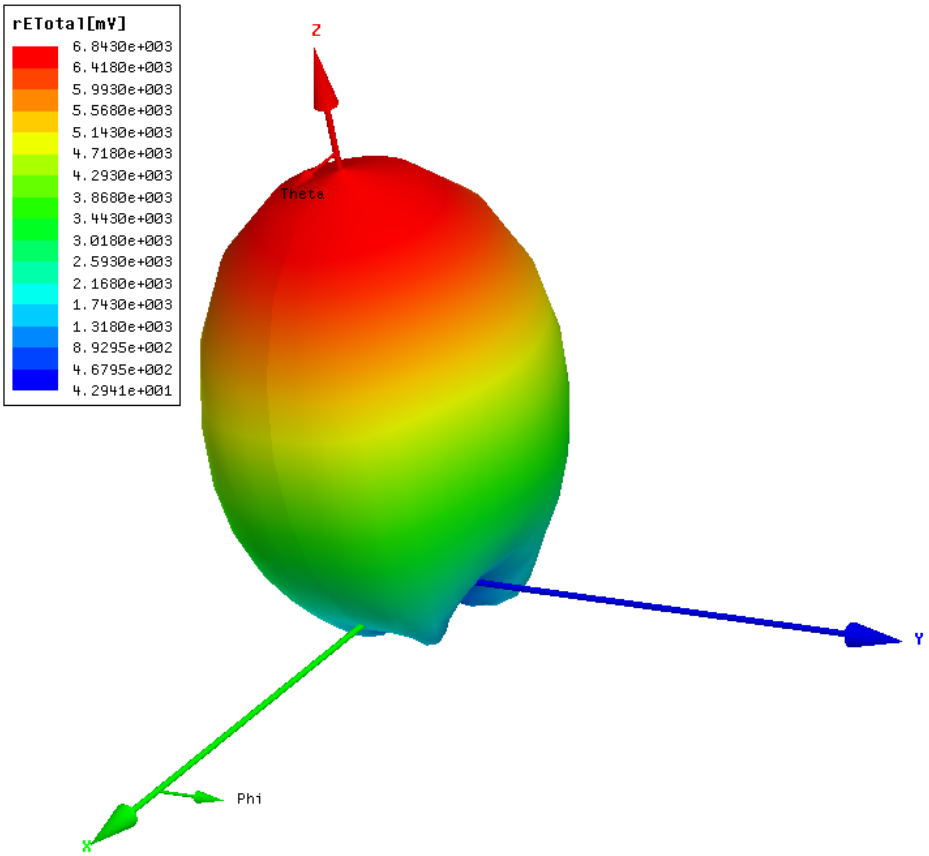

Figure 18: Radiation Pattern for Wave Zero Tag on Dielectric on Conductive Plate.

Design Modeling and Optimization:

To determine the effect of the dielectric material shape on the transmitted/received signal power, a dipole model was used. This was done to simplify HFSS simulation and is justified by the results of tag modeling in HFSS. All models use a material modeled after the CaTi K200 dielectric material from Morgan Technical Ceramics, which has a dielectric constant of 200. A box shaped dielectric inlay against a conductive plate was simulated in HFSS, shown in Figure 19. The box thickness is 228.34 mils, corresponding to $\lambda/4$ at a dielectric constant of 200. The box length and height were arbitrarily assigned to 300 and 425 mils respectively. All subsequent inlay design simulations may then be compared to this simulation to determine the effect of each alteration in inlay design on electric field intensity magnitude. Figure 20 shows the resulting radiation pattern with associated values of electric field intensity magnitude.

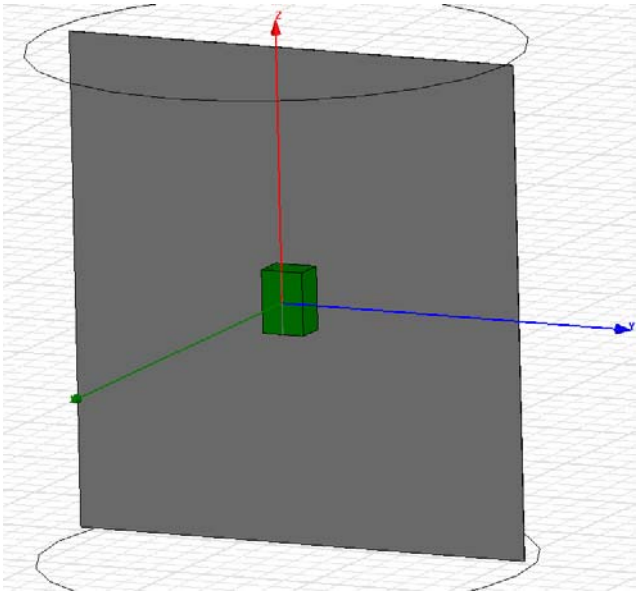

Figure 19: HFSS Model of Base Design, a dipole antenna on box shaped dielectric inlay attached to conductive plate.

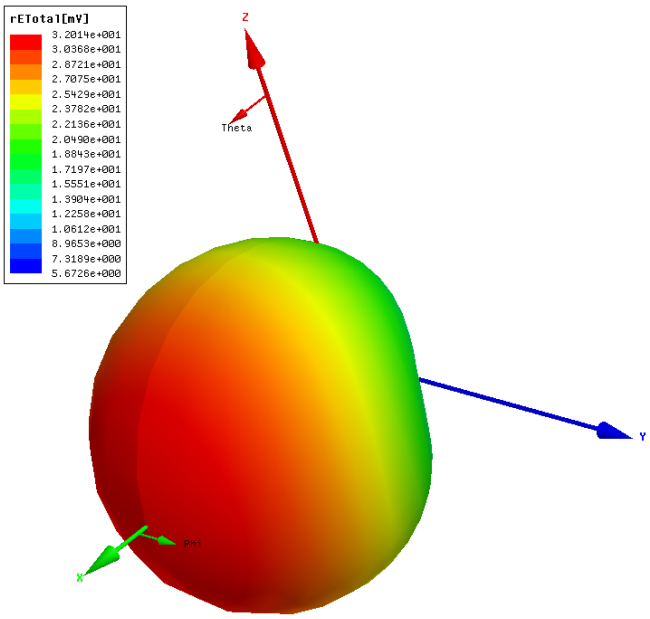

Figure 20: Simulated radiation pattern for Base Design with associated |E| values.

The first design alteration, Design 1 shown in Figure 22, was chosen to maintain a relatively constant travel distance through the dielectric material with respect to phi. Figure 20 shows a cross section of this design, demonstrating the travel distance through the material. The intention was to create a design less dependant upon reader location, useful in applications where the reader is not fixed. However, the resulting radiation pattern shown in Figure 23 displays nearly the same variation in E with respect to phi as that of the base design. In addition, the volume of Design 1 is greater than the Base Design volume, so more material would be required for the same signal power delivered to the reader. This is very important due to the high cost of high K dielectric materials. For this reason, Design 1 is inferior to the base design.

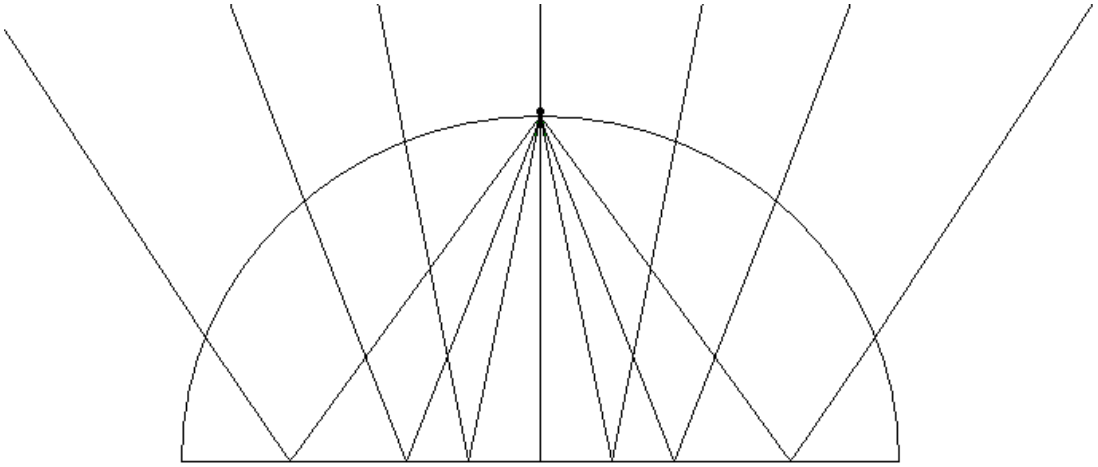

Figure 21: Reflection path through cross section of Design 1.

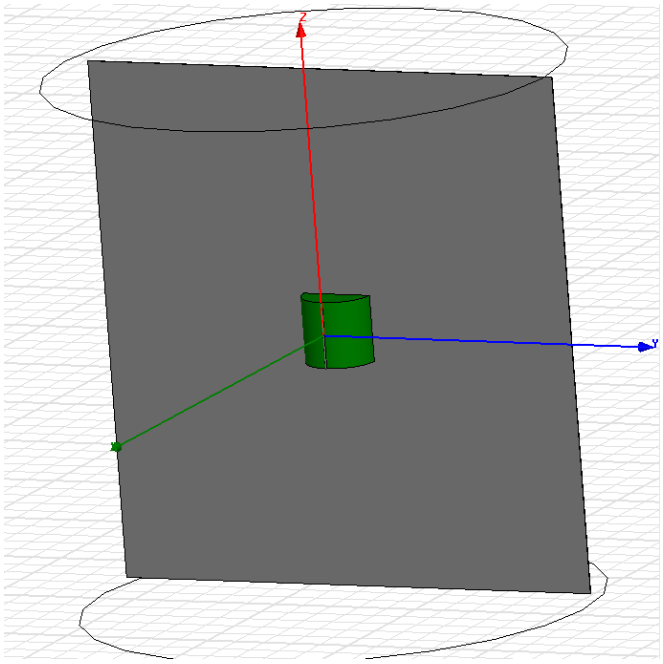

Figure 22: HFSS Model of Design 1.

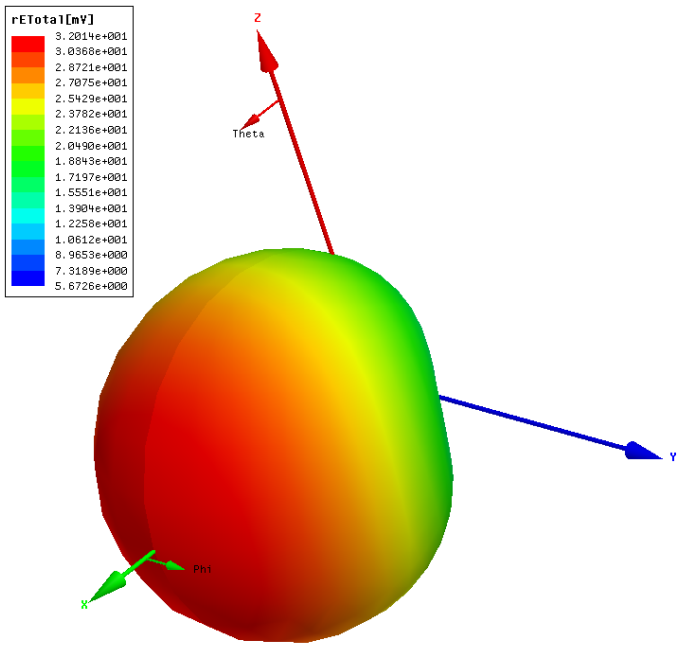

Figure 23: Simulated Radiation Pattern of Design 1.

The second design is a combination of a block and cylindrical shaped substrate. This design is modeled after the shape of the blue Omni ID tags used for outdoor applications. The block dimensions are the same as the Base Design, while the cylinder radius is 228.34 mils. Design 2 is shown in figure 24 while the radiation pattern is shown in Figure 25.

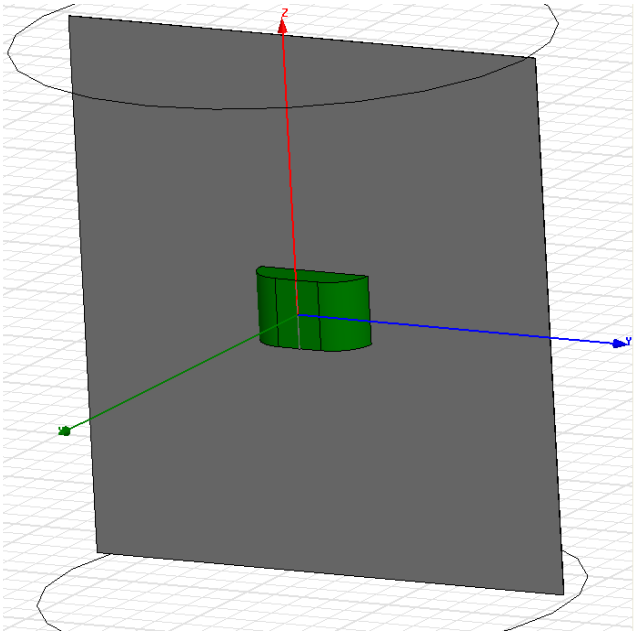

Figure 24: HFSS Model of Design 2.

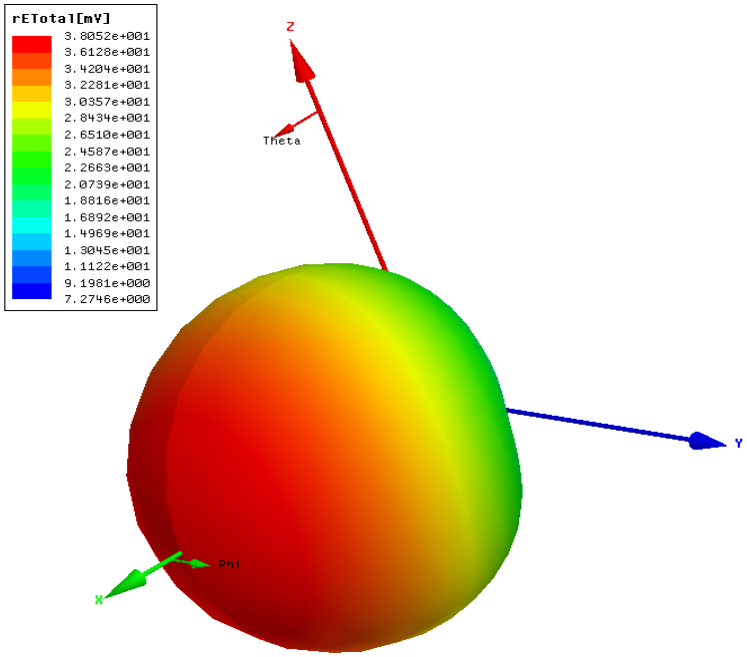

Figure 25: Simulated Radiation Pattern of Design 2.

Note that the maximum E field magnitude (x directed) is greater than that of the base design, and design 2 (Figures 20, 23). This shows that this design is an improvement upon the box shaped base design. The improvement is most likely the result of refraction of EM waves at the dielectric/air interface.

The third and final design, Design 3, is shown in Figure 26. It consists of a cylinder of radius 228.34 mils with two hemispheres at the top and bottom. The resulting radiation pattern is shown in Figure 27.

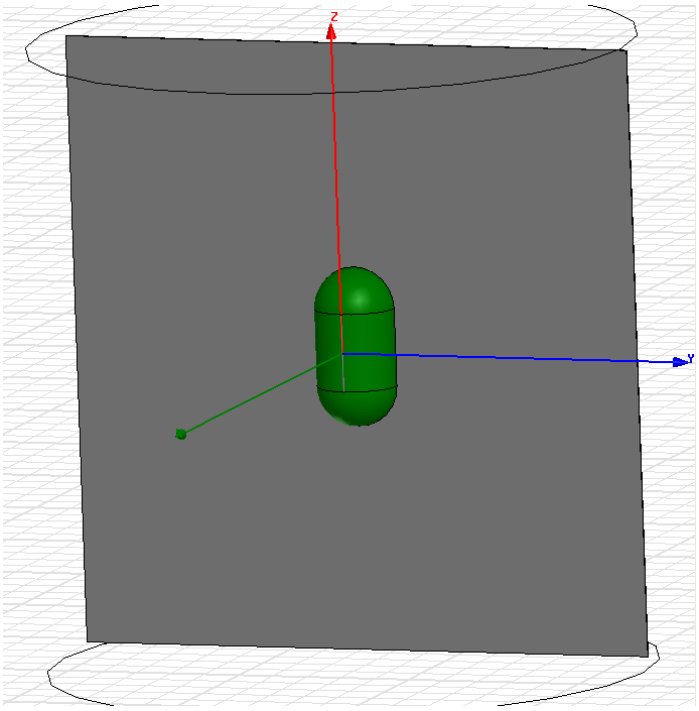

Figure 26: HFSS model of Design 3.

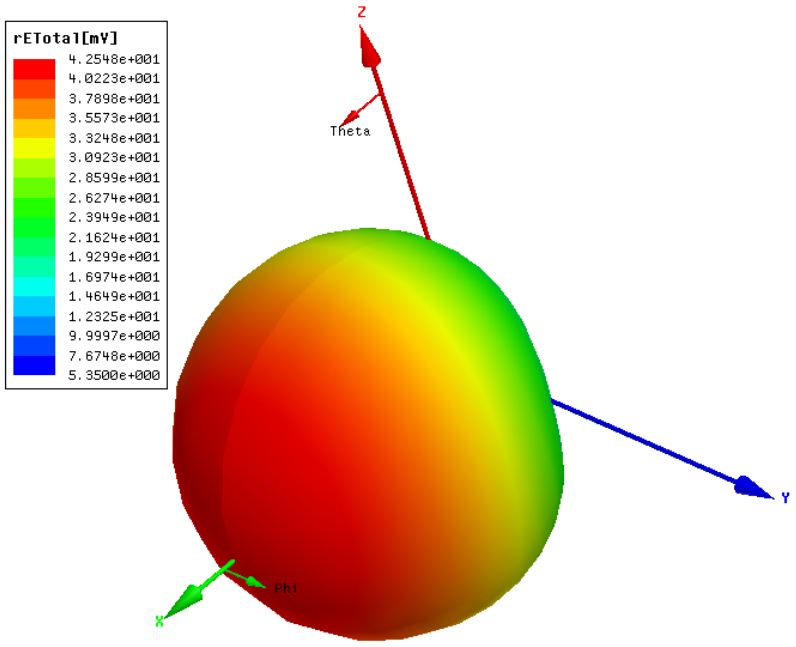

Figure 27: Simulated Radiation Pattern of Design 3.

The electric field intensity magnitude in the x direction of Design 3 is much higher than that of the Base Design, Design 1, or Design 2. Table 4 shows the values of electric field intensity magnitude in the x direction, or direction of the reader, as well as volume of each design to determine the relative material cost. The relative volume and $|E|_{max}$ relative to the Base Design are also shown.

Design	Volume (in^3)	$\|E\|_{max}$ (mV)	Rel. Volume	Rel. $\|E\|_{max}$ (%)
Base Design	0.02911	3.201	1	1
Design 1	0.03685	3.201	1.266	1
Design 2	0.06596	3.805	2.266	1.188
Design 3	0.06178	4.255	2.122	1.329

Table 3: Design Modeling Results

Conclusions and Recommendations:

Design 3 (Figure 21) was determined to be the optimum design in terms of maximum electric field intensity delivered to the reader. While these changes in design form the box shaped Base design (Figure 14) result in improvements in tag operation such as increased signal power delivered to the reader and maximum read distance, it comes at the cost of additional dielectric material. Due to the high cost of high K dielectric materials (cost generally increases with relative permittivity), this tradeoff is generally not cost effective. If the application requires greater received signal power or read distance, the larger Flex Omni ID tags could be used, or perhaps an active RFID tag could be used if the application permits However, Design 3 did offer greater $|E|_{max}$ while having less volume than Design 2, modeled after the Omni ID ABS tag. Unless the design of the ABS tag is essential to its function in "harsh" environments, Omni ID could investigate the possibility of a change in design of the ABS tag for applications with greater read distance.

Continued Research:

Due to an error in the Labview software, and lack of time to debug the error, testing of Design 3 was not possible. The reader was functioning within the program, and the program displayed incrementing attenuation. However, increased attenuation had no effect on the number of successful reads. Therefore, the error must lie in the function block that increments the attenuator or the attenuator itself is faulty. After the error is fixed, Design 3 can be tested using the same method as used in RFID characterization. The resulting radiation pattern can then be compared to the Base Design to determine an improvement in received signal power.

References:

1. Labview Computer Software. Vers. 8. Austin, TX: National Instruments, 2009
2. HFSS Computer Software. Vers. 11. Pittsburgh, PA: Ansoft 2009

Parts List:

Part Name	Cost
Alien RFID sample pack	Donated
Wave Zero RFID sample pack	Donated
Omni ID tag evaluation pack	Donated
HFSS Computer Software	Licensed by Cal Poly
Alien RFID reader 9800	Donated
Total	$0

Schedule:

Task	Length	Start date	End Date
Research	2 weeks	March 30, 2009	April 10, 2009
Procedure Testing	2 weeks	April 13, 2009	April 24, 2009
Alien Tag Testing	2 weeks	April 27, 2009	May 8, 2009
Omni ID Tag Testing	3 weeks	May 11, 2009	May 29, 2009
Design Simulation	4 weeks	Sept 28, 2009	Oct 23, 2009
RFID Modeling	3 weeks	Oct 26, 2009	Nov 13, 2009
Report	4 weeks	Nov 16, 2009	Dec 11, 2009